Numerical investigation of free convection within a circular cavity with a flexible fin

Atika Bencherif[1], Mohamed Bouzit[1], Abderrahim Mokhefi[2], Hanaa Derraz[1] and Fatima Zohra Khelif[1]

[1]*Laboratory of Maritime Sciences and Engineering LSIM Faculty of Mechanical Engineering, University of Science and Technology of Oran Mohamed Boudiaf, Oran, Algeria*
[2]*Mechanics, Modeling and Experimentation Laboratory L2ME, Faculty of Sciences and Technology, Bechar University, Bechar, Algeria*

Abstract

The problem of unsteady natural convection inside a circular cavity containing a flexible fin is numerically studied in this work. The cavity's left side is hot, while the right side is cold. A flexible elastic fin is attached to the center of the hot wall. The fluid-structure interaction in the cavity and flexible fin is combined with Newtonian fluid. The governing equations of the fluid-flexible fin interaction are solved using the Finite Elements method and the arbitrary Lagrangian-Eulerian approach. The effects of an elastic flexible fin on natural convection within circular cavities were investigated in this study. The Rayleigh number ($10^3 \leq Ra \leq 10^5$) and Elasticity modulus ($10^{10} \leq Et \leq 10^{11}$) are the parameters studied, the average Nusselt numbers well as isotherms and streamlines, are investigated. The results show that increasing the Rayleigh number causes an increase in the average Nusselt number, which becomes significant for a higher Rayleigh number. Therefore, it is discovered that the circular shape of the cavity may improve the heat transfer rate.

Keywords: Newtonian fluid; fluid-structure interaction; finite elements method; elasticity modulus; average Nusselt number; Rayleigh number.

Available on-line at the Journal web address: http://www.ache.org.rs/HI/

ORIGINAL SCIENTIFIC PAPER

UDC: 551.509.313:631.436.1

Hem. Ind. **79(1)** 31-46 (2025)

1. INTRODUCTION

Heat transfer by natural convection in obstructed cavities is of both fundamental and industrial importance, finding applications in various fields including electronic equipment cooling, solar collector manufacturing, housing thermal management, and nuclear engineering. In recent years, extensive experimental and numerical research has been dedicated to understanding heat transfer in cavities equipped with fins.

Considering natural convection, many published works have investigated the problem of unsteady fluid-structure interaction inside various cavities, such as square cavities [1-3], circular enclosures [4], and L-shaped enclosures [5]. Additionally, several studies have explored mixed convection across different enclosures, including those with multiple openings [6], channel configurations [7], and flexible walls [8].

Further research has aimed to better comprehend this phenomenon by considering different fluids, including Newtonians, non-Newtonians, and nanofluids. For instance, many studies on Newtonian fluid natural convection have examined the effects of oscillating flexible fins [9-11] indicating an increase in the fluid flow rate amplitude with increasing fin-free end amplitude. Additionally, the heat transfer rate in the case of using of flexible fins has shown a higher Nusselt number compared to that determined when using rigid fins. Raisi *et al*. [12] presented the effect of fluid-solid interaction on transient natural convection inside a square cavity and discovered that the impact of increasing baffle length on the thermal performance of the cavity varies based on the Rayleigh number and the rigidity or flexibility of the system. Heat transfer properties in cavities with porous mediums have been also studied [13-16]. The findings

Corresponding author: Atika Bencherif, Laboratory of Maritime Sciences and Engineering LSIM Faculty of Mechanical Engineering, University of Science and Technology of Oran, Mohamed Boudiaf, Algeria
E-mail: atika.bencherif@univ-usto.dz
Paper received: 29 October 2023; Paper accepted: 4 February 2025; Paper published: 17 April 2025.
https://doi.org/10.2298/HEMIND231029001B

indicate that an oscillation amplitude of 0.1 significantly improves the heat transfer rate across all Rayleigh numbers, and the average Nusselt number is typically greater for Darcy models than for Darcy-Forchheimer models. A study of natural convection heat transfer in buoyancy-induced flow scenarios within a square cavity [17] has shown that in the scenario of a plate fixed at its top, the highest stress is observed with an inclination angle of 40°. In a recent study, natural convection around square cylinders and within enclosures containing heated circular cylinders has provided insights into optimal heat transfer conditions [18]. It was observed that the 45° angle of the rotation square cylinder provides the optimal and the most efficient heat transfer at a higher Rayleigh number. Investigation of unsteady natural convection heat transfer within an enclosure with a heated circular cylinder [19,20] has indicated that the enclosure performance rate is the highest when the membrane is placed at 45°, while the increase in the Prandtl number (from 0.1 to 0.2) leads to the decrease in the Nusselt number, even though the Rayleigh number is increasing. Furthermore, numerical methods such as the smoothed particle element method (SPEM) have been proposed to effectively model fluid-structure interactions in free surface problems [21]. Heat transfer enhancement in a vented cavity using an externally oscillating flexible flow modulator has been demonstrated [22], showing the increase in heat transfer as the oscillation period of the flexible modulator decreases. A numerical approach utilizing the sharp-interface CURVIB solver (curvilinear immersed boundary solver) has been employed to simulate fluid-structure interaction (FSI) problems in complex domains involving thin, flexible solid structures [23].

Investigations of natural convection of a non-Newtonian power-law fluid with utilization a flexible fin [24-26], indicated that the fin predominantly deforms in dilating non-Newtonian fluids, while rigid fins are experiencing higher maximal stresses as compared to flexible fins. Additionally, a significant decrease in the average Nusselt number is observed when the plate length is reduced. In other studies, laminar natural heat transfer was investigated for non-Newtonian power-law fluids within different enclosure geometries such as a square enclosure [27,28], rectangular enclosure [29,30], and an enclosure with a heated hexagonal block [31] as it was summarized in [37]. The compressible B-spline material point method (Weakly Compressible BSMPM) was provided and extended to resolve the complicated free surface flow of a non-Newtonian fluid following a power law rheology model [32]. Pandey *et al*. [33] examined thermal and flow characteristics of non-Newtonian fluids at Ra = 10^7 in a circular cylinder within a square cavity. They concluded that heat transfer significantly increased for cases of a pseudoplastic fluid (n <1) compared to cases of a dilatant fluid (n> 1). Numerical simulation of convective heat transfer and flow in a non-Newtonian power-law fluid was performed using the lattice Boltzmann method [34] showing that as the flow behavior index increases for a given Rayleigh number, the average Nusselt number at the hot wall and the rate of melting decrease. Jain *et al.* [35] investigated the heat transfer and flow characteristics of natural convection from a hot cylinder body in a square enclosure, and the results showed ~11% increase in heat transfer for an arc radius approaching 0 mm. The investigation of natural convection in a non-Newtonian fluid within a cavity is conducted over time, focusing on controlling parameters such as Rayleigh number, power-law index, and side oscillation frequency [36]. The smoothed particle hydrodynamics (SPH) method was used to simulate natural convection in a differentially heated square cavity at high Rayleigh numbers when the chaotic motion has a significant influence on the heat transfer characteristic [38].

In summary, research has addressed natural convection within various enclosure geometries using advanced numerical methods, shedding light on fundamental heat transfer phenomena. The purpose of this study is to investigate the effects of an elastic flexible fin on natural convection in a Newtonian fluid within a circular cavity, considering fluid-structure interactions.

2. MODELING APPROACH

Geometry considered in the current study is a circular cavity with a flexible fin attached to the central part of the hot left wall, as shown in Figure 1. The right wall is maintained cold at a temperature T_c*, while the left wall is brought to a higher temperature T_h*. The fluid circulating in the cavity is considered Newtonian and incompressible, while the flow is laminar and two-dimensional.

Based on these assumptions and the arbitrary Lagrangian-Eulerian (ALE) approach, the equations representing the hydrodynamic and thermal features of the problem are stated as follows, Equations. (1) to (7).

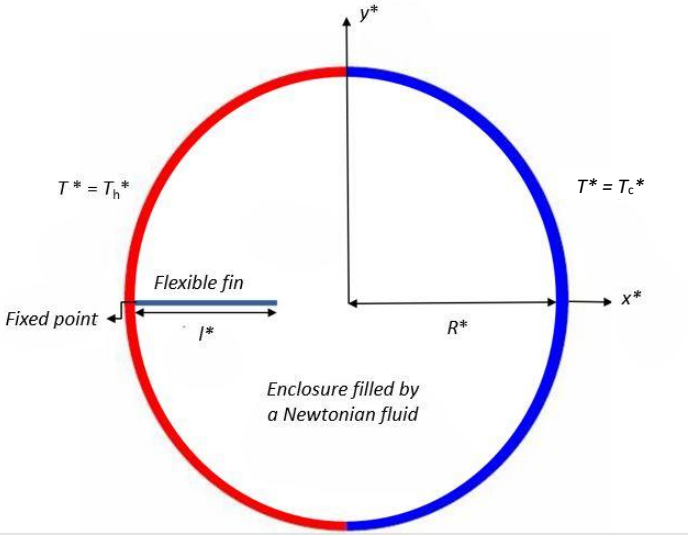

Figure 1. Physical model of convection in a cavity with a flexible fin and coordinate system where T represents the dimensional temperature field, (x*, y*) shows the dimensional Cartesian coordinate system, R* and l* represent the dimensional characteristic size of the cavity and the length of the flexible fin, respectively*

Continuity equation:

$$\nabla^*\mathbf{u}^*=0 \tag{1}$$

Momentum equations:

$$\rho_f\left[\frac{\partial \mathbf{u}^*}{\partial t}+\left(\mathbf{u}^*-\mathbf{w}^*\right)\nabla^*\mathbf{u}^*\right]-\nabla^*\left[-P^*I+\mu\left(\nabla^*\mathbf{u}^*+\left(\nabla^*\mathbf{u}^*\right)^{tr}\right)\right]-\rho_f\beta\mathbf{g}\left(T^*-T_c^*\right)=0 \tag{2}$$

The energy equation for the fluid:

$$\left(\rho c_p\right)_f\left[\frac{\partial T^*}{\partial t}+\left(\mathbf{u}^*-\mathbf{w}^*\right)\nabla^*T^*\right]-k_f\nabla^{*2}T^*=0\cdot \tag{3}$$

For the elastic structure domain, the energy equation for the fin can be written as:

$$\left(\rho c_p\right)_f\frac{\partial T^*}{\partial t}-k_s\nabla^{*2}T^*=0\cdot \tag{4}$$

where **u*** represents the velocity vector, **w*** shows the moving mesh velocity vector, and *P* represents the pressure field, *I* represent the identity tensor, *tr* is the transpose of a matrix, **g** is the gravity vector, α and β represent the thermal diffusivity and volumetric thermal expansion respectively, ρ is the density, c_p is the specific heat at constant pressure, k_f and k_s signify the thermal conductivity of the fluid and the solid, respectively.

The Neo-Hookean solid model is applied to express the stress tensor σ^*:

$$\sigma^*=J^{-1}FSF^{tr}\,\big|F=(I+\nabla^*\mathbf{d}_s^*),\ J=\det(F)\text{ and }S=\partial W_s/\partial\varepsilon\cdot \tag{5}$$

$$W_s=\frac{1}{2}I(J^{-1}I_1-3)-I\ln J+\frac{1}{2}\lambda(\ln J)^2\,\Big|\begin{matrix}I=E/(2(1+\nu))\\ \lambda=E\nu/((1+\nu)(1-2\nu))\end{matrix}. \tag{6}$$

$$\varepsilon=\frac{1}{2}\left(\nabla^*\mathbf{d}_s^*+\nabla^*\mathbf{d}_s^{*tr}+\nabla^*{}_s^{*tr}\nabla^*\mathbf{d}_s^*\right)\cdot \tag{7}$$

where *F* is the deformation gradient tensor, F^{tr} is the transpose of the deformation gradient tensor, d_s^*represents the solid displacement vector, *S* the second Piola-Kirchhoff, W_s is the strain energy density function, I_1 represents the first invariant of the right Cauchy–Green deformation tensor, *E* the young's modulus of the solid, *v* the poisson's ratio of the solid, ε is the strain.

Boundary conditions applicable to the external walls Eqs. (8) and (9), and the flexible fin interface Eq. (10) are expressed as:

At the hot wall:

$T^* = T_h^*$, $\mathbf{u}^* = v^* = 0$ (8)

At the cold wall

$T^* = T_c^*$, $\mathbf{u}^* = v^* = 0$ (9)

At the interface of the flexible fin:

$$k_f \left.\frac{\partial y}{\partial x}\right|_f = k_s \left.\frac{\partial y}{\partial x}\right|_s . \quad (10)$$

This equation ensures that the heat flux leaving the fin is equal to the heat flux entering the substrate, where y typically represents temperature, which is a function of the position (x) in this case.

Also, the Rayleigh and Prandtl numbers (Ra and Pr, respectively) and the elasticity modulus (E_τ) are introduced as:

$$\mathrm{Ra} = \frac{\rho_0^{\,2} c_p \mathbf{g} \beta \Delta T 2R^3}{\mu_B k} . \quad (11)$$

$$\mathrm{Pr} = \frac{c_p \mu_B}{k} . \quad (12)$$

$$E_\tau = \frac{E 2R^{*2}}{\rho_f \alpha_f^{\,2}} . \quad (13)$$

To quantify the heat transfer between the flexible fin and the fluid, we used the Nusselt number as follows in the Eqs. (14) and (15):

$$\mathrm{Nu}_f = -\frac{\partial \theta}{\partial X} . \quad (14)$$

$$\mathrm{Nu}_s = -k_r \frac{\partial \theta}{\partial X} . \quad (15)$$

Nu_f quantifies the heat transfer rate at the interface between the flexible fin and the surrounding fluid, and the Nu_s describes the heat transfer within the fin material. θ represents the dimensionless temperature, X is a dimensionless spatial coordinate along the fin, and k_r represents the thermal conductivity ratio.

The average Nusselt number on the wall is presented as follows:

$$\overline{\mathrm{Nu}} = \int_0^{s_1} \mathrm{Nu}_f dy + \int_{s_1}^{s_2} \mathrm{Nu}_s dy + \int_{s_2}^{1} \mathrm{Nu}_f dy \Bigg|_{\substack{s_1 = \frac{1}{2} - \frac{t_{fin}}{2} \\ s_2 = \frac{1}{2} + \frac{t_{fin}}{2}}} . \quad (16)$$

where s_1 and s_2 represent the positions along the wall based on the thickness of the fin.

3. NUMERICAL METHOD, GRID STUDY AND VALIDATION

3. 1. Numerical approach and mesh independency

The governing equations and boundary conditions are transformed into weak form before being numerically solved in the moving grid system using the finite element method. An Arbitrary Lagrangian-Eulerian (ALE) method for fluid-flexible fin interaction is utilized. The computational domain is discretized into triangular non-uniform elements as shown in Figure 2. To simplify the nonlinear terms in the momentum equations, a Newton iteration algorithm is used. Physical and thermal properties of the fin and fluid adopted for simulations are shown in Table 1.

The equations are solved using the finite element method. The process starts by defining physics, PDEs, and boundary conditions, followed by mesh generation and discretization. The system is then assembled into a global matrix ($Ax = b$) and solved using iterative solvers.

In numerical methods for solving physical problems, grid-independence tests are achieved to confirm that the results are independent of the number of mesh elements. Table 2 examines the average Nusselt number (Nu_{avg}) on the hot wall at Ra = 10^5, Et = 10^{10}, and Pr = 10 for five different mesh sizes. Table 2 shows the number of elements used in the

fluid domain and the Nusselt number for various mesh sizes at a steady state. As a result, it can be determined that the grid with 245180 elements (case 4) is appropriate for use in all the computations in this paper.

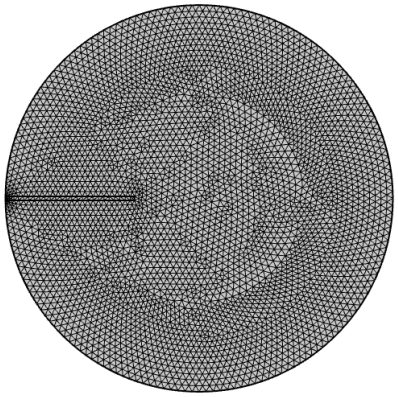

Figure 2. The schematic presentation of the utilized grid

Table 1. Physical and thermal properties of materials

Material	Physical properties	Thermal properties	Dimensionless parameters
Fluid	ρ_f = 1000 kg m^{-3} μ_f = 1.457 Pa s	α = 0.14627 mm^2 s^{-1} k_f = 0.609 W m^{-1} K^{-1} C_p = 4179 J kg^{-1} K^{-1} β = 1.2E-7 K^{-1}	Pr =10 Fv = 0 k_r = 100 ρ_r = 1
Fin	ρ_s = 1500 kg m^{-3} t_{fin} = 0.226 mm	k_s = 1000 W m^{-1} K^{-1} C_p = 100 J kg^{-1} K^{-1}	

Table 2. The average Nusselt number at the steady state solution for different grids when Et = 10^{10}, Ra = 10^5 and Pr = 10

Grid	Number of elements	Time, s	Nu_{avg}
Case (1)	63154	2012	7.96685
Case (2)	110656	3910	8.07652
Case (3)	171800	5846	8.16314
Case (4)	245180	8573	8.22831
Case (5)	332260	11679	8.22837

3. 2. Validation with others results

Another critical step in the simulation to ensure the accuracy and correctness of the obtained results is the validation through other studies. This work is validated on the basis of a study reported in literature [24]. In the literature [24], the study focused on the flow and heat transfer of a power-law non-Newtonian fluid within a cavity, driven by buoyancy forces. The interaction between the non-Newtonian flow in the cavity and the hot fin was modeled through Fluid-Structure Interaction (FSI), where the flow caused the fin to deform, which subsequently influenced both the flow and heat transfer. This two-way coupling was simulated using the Arbitrary Lagrangian-Eulerian (ALE) method with a moving mesh, while the governing equations were solved by using the finite element method.

First, the findings of this investigation are compared to the contours of isotherms obtained in that study [24] when Pr = 10 and Et = 10^{10} have been used for the validation of this study. As shown in Figure 3, the present numerical results are in thorough agreement with the literature results [24].

Second, streamlines reported in literature [24] when Pr = 10 and Et = 10^{10} are compared for different Rayleigh numbers (Ra) with those obtained by the present method (Fig. 4), showing satisfactory agreement.

Finally, for validation of the natural convection mechanism of a Newtonian fluid within a cavity, numerical modeling in the reference [24] has been re-simulated by the code employed in the present study. The evaluation of the Nusselt number for different values of the Rayleigh number (Ra) is represented in Table 3, showing satisfactory agreements of the results.

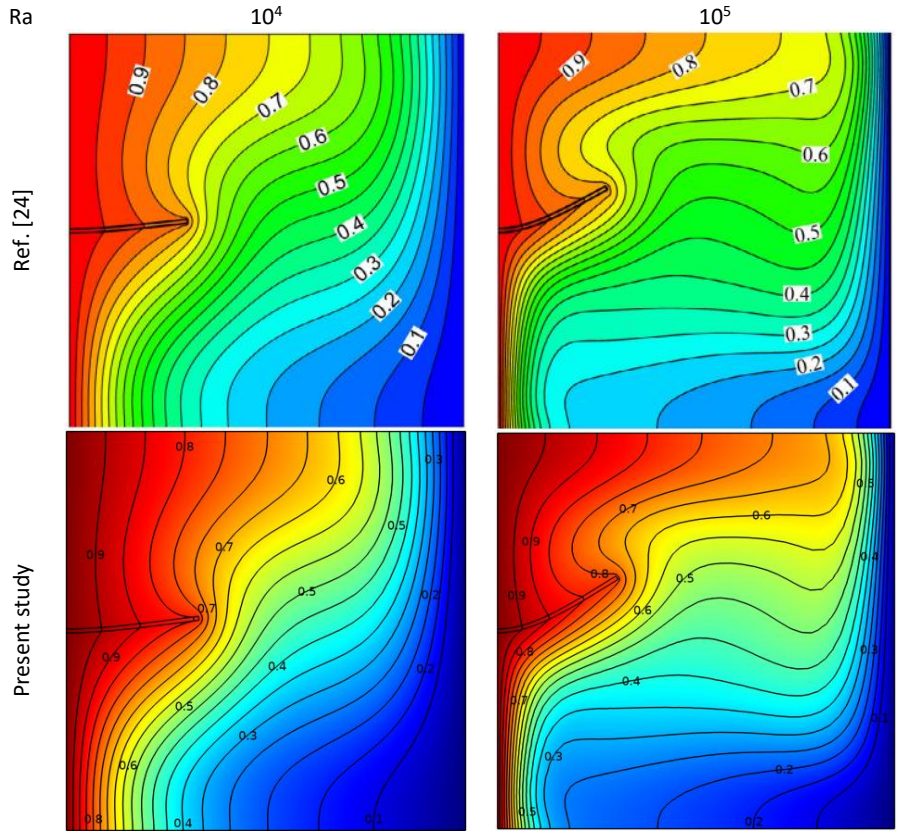

Figure 3. Comparing the results of the present study and the contours of isotherms reported by in literature [24] when Pr = 10 and Et = 10^{10}

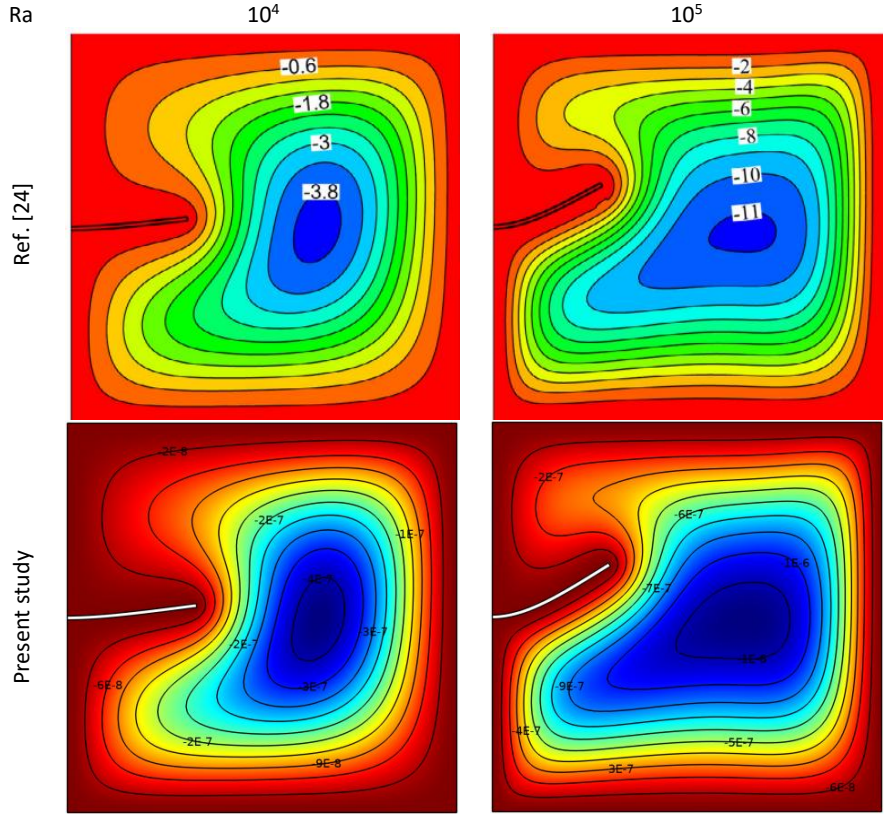

Figure 4. Comparison of the results obtained in the present study and the streamlines reported in literature [24] when Pr = 10 and Et = 10^{10}

Table 3. The average Nusselt (Nu) for different values of the Rayleigh number at Pr =10

Ra	Nu_{avg}		Error, %
	Shahabadi *et al.* [24]	Present study	
10^3	1.11883	1.12423	0.480
10^4	1.92385	1.92536	0.784
10^5	4.41245	4.41632	0.387

4. RESULTS AND DISCUSSION

This study examines the impact of various factors on thermo-flow fields and deformation of an elastic fin. The factors under investigation include the Rayleigh number ($10^3 \leq Ra \leq 10^5$), and the elasticity modulus ($10^{10} \leq Et \leq 10^{11}$). This research aims to inform readers about the consequences of different parameters on the behavior of the fin.

Figure 5 illustrates the changes in isotherms over time in a scenario with $Ra = 10^5$, $Pr = 10$, and $Et = 10^{10}$.

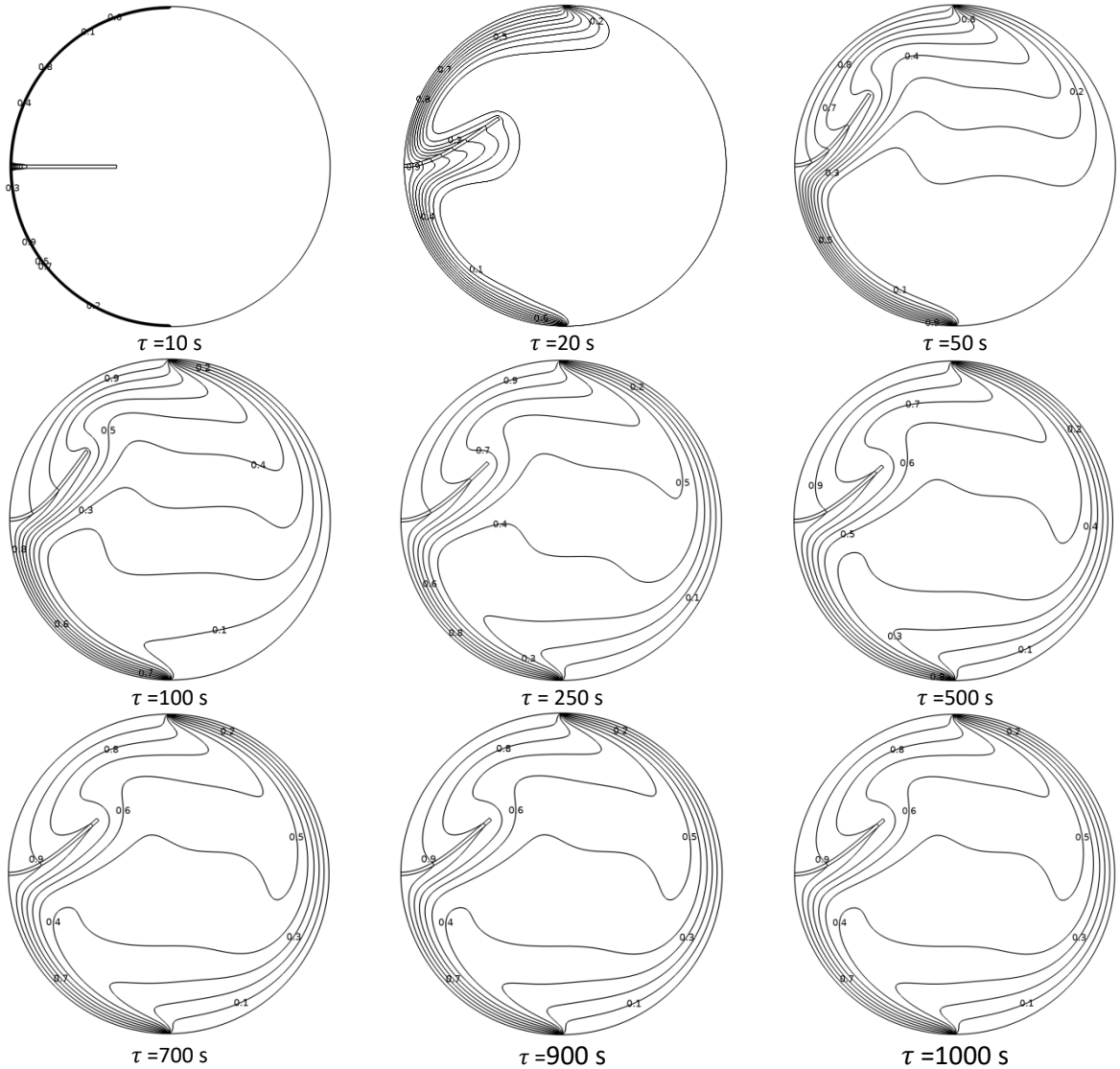

Figure 5. Development of isotherms and deformation of the flexible fin overtime (τ) for Ra = 10^5, Pr = 10, and Et = 10^{10}

Initially, at overtime τ = 10 s, the flexible heat-conducting fin remains stationary due to the dominance of conduction in heat transfer. As time progresses to τ = 20 s, there is a noticeable flow of fluid and heat transfer, causing the flexible fin to move towards the hot wall. Between 50 s < τ < 250 s, more vortices appear around the fin, leading to a shift in the isotherms towards the fin. Consequently, the role of convection becomes more significant compared to conduction in

the heat transfer mechanism. Finally, in the steady state at τ = 1000 s, the fin movement aligns with the flow direction, leading to rotational flows in the upper left wall. This convection cell exhibits the highest circulation intensity among all-time instances. It can also be observed that the flexible fin reaches its highest level of displacement during this period.

Figure 6 shows an evolution of the streamlines with time at Ra = 10^5, Pr =10 and Et = 10^{10}. According to this figure, two weak vortices are seen at the initial time above and under the fin on the hot wall due to the negligible convective heat transfer. As time passes, we can see one vortex under the fin close to the left wall. In the time period 500 s <τ< 1000 s, there are two weak vortices: one vortex is next to the cold wall, and another is on the hot wall.

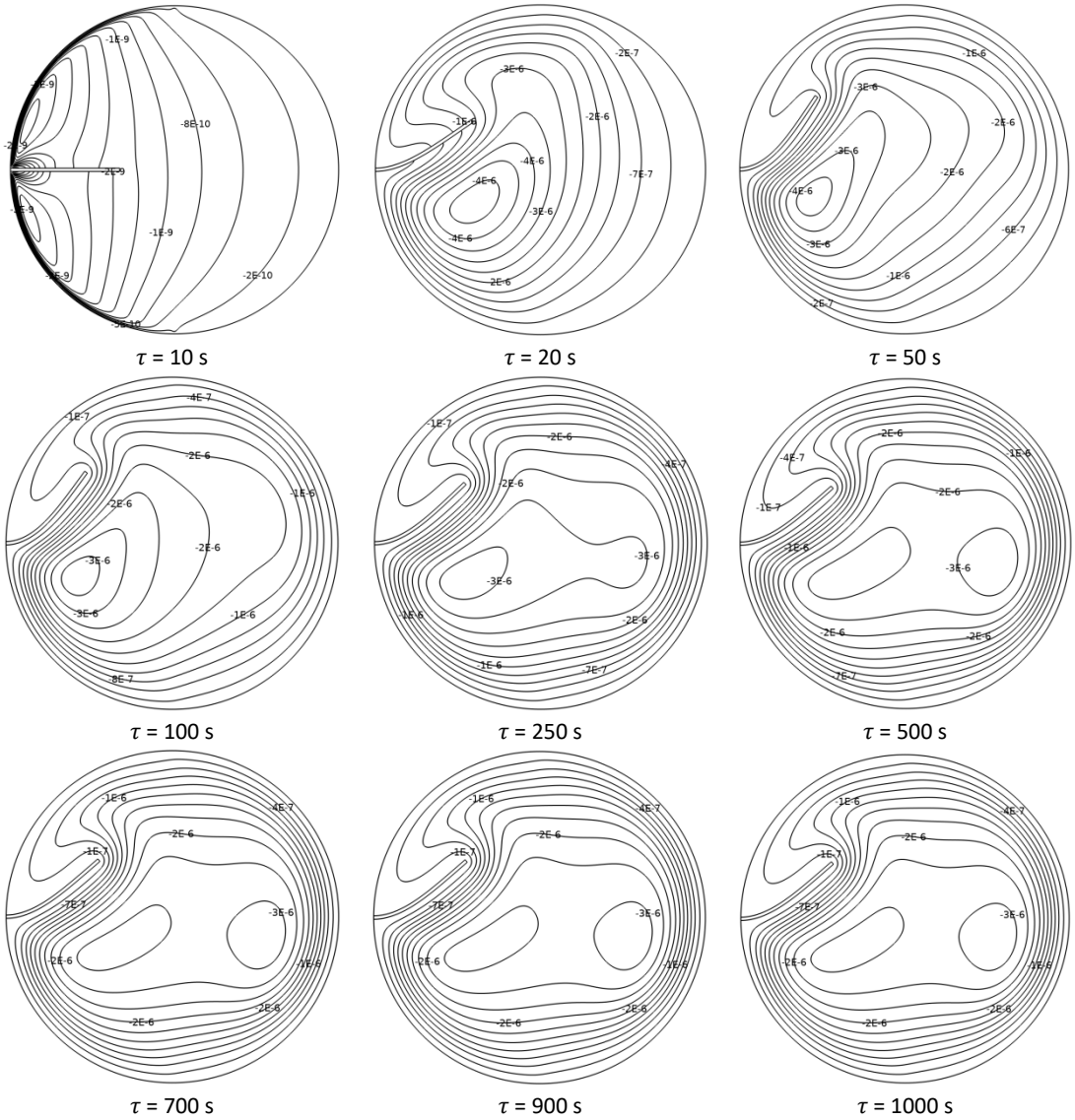

Figure 6. Development of streamlines and deformation of the flexible fin overtime for Ra = 10^5, Pr = 10 and Et = 10^{10}

Figure 7 displays the effects of elasticity modulus (Et) and different values of the Rayleigh number (Ra) on the isotherms at the steady state at Pr = 10. According to the figure, at the lower Rayleigh number (Ra = 10^3), the elastic fin is not moving. Meanwhile, the isotherms are parallel to the cold and hot vertical walls of the cavity, indicating that conduction is the main mechanism of heat transfer. In the case of increasing the Rayleigh number *i.e*. Ra = 10^4, motion of the fin is solely affected, and natural convection becomes more intense. In addition, the increase in the Rayleigh number indicates that the isotherms are deviating from the vertical state, and the buoyant-driven flow is beginning to dominate the heat transfer mechanism. At the higher Rayleigh number of Ra = 10^5, natural convection is the main heat

transfer mechanism. It is interesting to note that the motion of the fin mostly affects the upper left hot wall for a lower elasticity modulus of Et = 10^{10}. The reason for this behavior could be the increase in the convective flow.

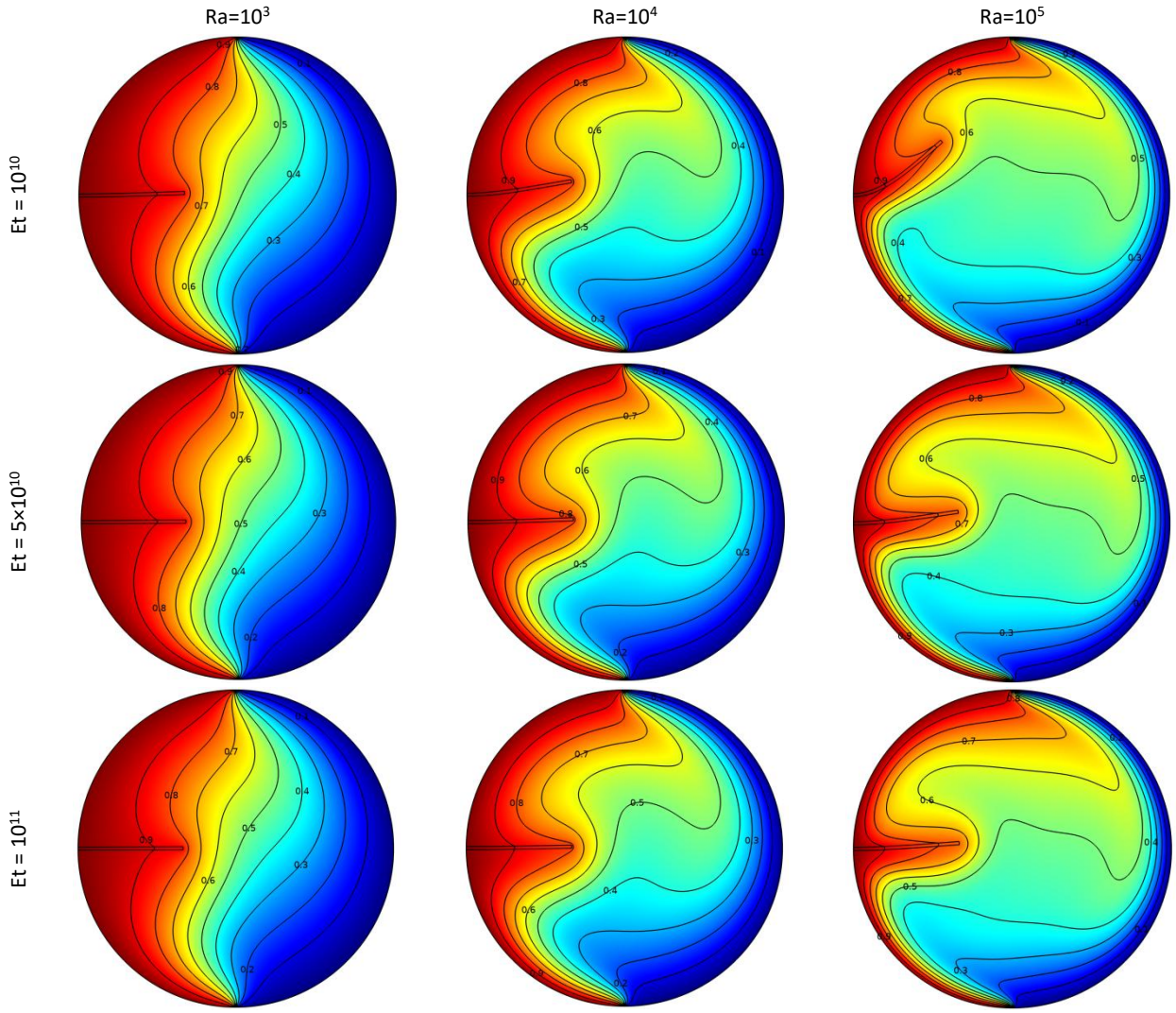

Figure 7. Isotherm contours for various Rayleigh numbers (Ra) and different values of elasticity modulus (Et) at Pr = 10

The results of the isothermal and steady-state streamlines at Pr = 10 and for various values of the Rayleigh number and elasticity modulus are shown in Figure 8. According to the figure, at a lower Rayleigh number (Ra = 10^3), the streamlines are symmetrical relative to the vertical centerline and the streamline pattern indicates that conduction is the main mechanism of heat transfer. At a Rayleigh number of Ra = 10^4, the streamlines become asymmetric regarding the vertical centerline, and a lateral vortex formed on the sides of the ribs moves to the right side of the cavity. Further, a double-eye circulation for a lower elasticity modulus (Et = 10^{10}) is depicted for a higher Rayleigh number of Ra = 10^5. The two vortices are central, and there is one vortex under the flexible fin close to the hot wall and another one next to the cold wall of the cavity. It is worth mentioning that vortices are less pronounced near the left upper portion of the fin, which rotates in counterclockwise direction, compared to other regions of the fin where vortices are more prominent.

Figure 9 shows the average Nusselt number overtime for different Rayleigh numbers at Et=10^{10} and Pr = 10. The average Nusselt number was the highest for Ra = 10^5 as compared to those determined for the other two Rayleigh numbers (*i.e.* 10^4 and 10^3). It is interesting to note that the average Nusselt number increases as the Rayleigh number is increased.

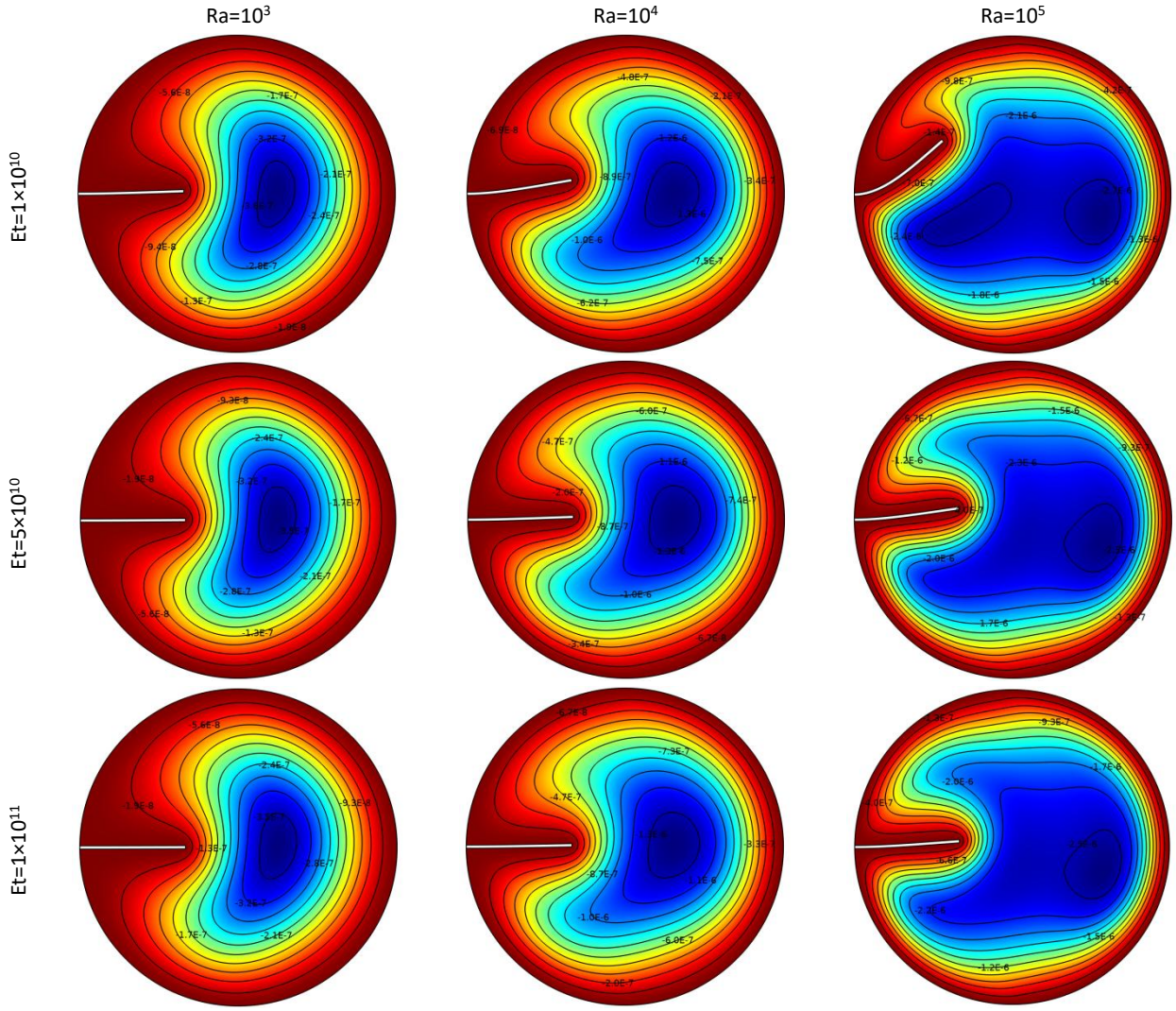

Figure 8. Streamline contours for various Rayleigh numbers (Ra) and different values of elasticity modulus (Et) at Pr = 10

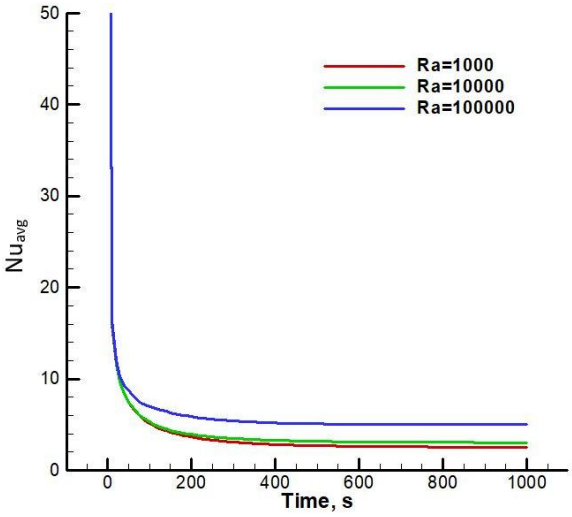

Figure 9. The average Nusselt number along the hot wall over time for different Rayleigh numbers at Et = 10^{10} and Pr = 10

Figure 10 presents the average Nusselt number on the hot wall over time for different values of elasticity modulus at Ra =10^5 and Pr = 10. This number decreases as the elasticity modulus reduces. Globally, the elasticity modulus has a

negligible effect on the average Nusselt number. The higher average Nusselt number is seen at the steady state for the highest elasticity modulus (Et = 10^{11}).

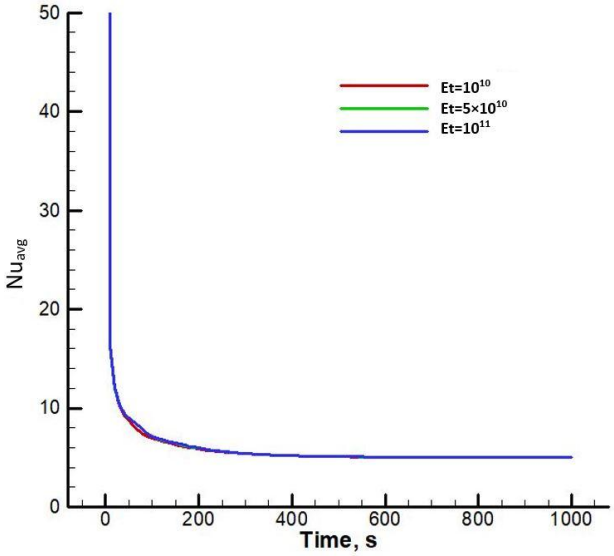

Figure 10. The average Nusselt number (Nu_{avg}) along the hot wall over time for different elasticity modulus at Et = 10^{10} and Pr = 10

Figure 11 shows the velocity magnitude along the vertical centerline of the cavity at the steady state for different Rayleigh numbers at Et = 10^{10} and Pr = 10. The maximal velocity values were observed in the fluid near the lower and upper walls at the highest Rayleigh number. Notably, lower velocity values can be seen at the level of the flexible fin for all Rayleigh numbers.

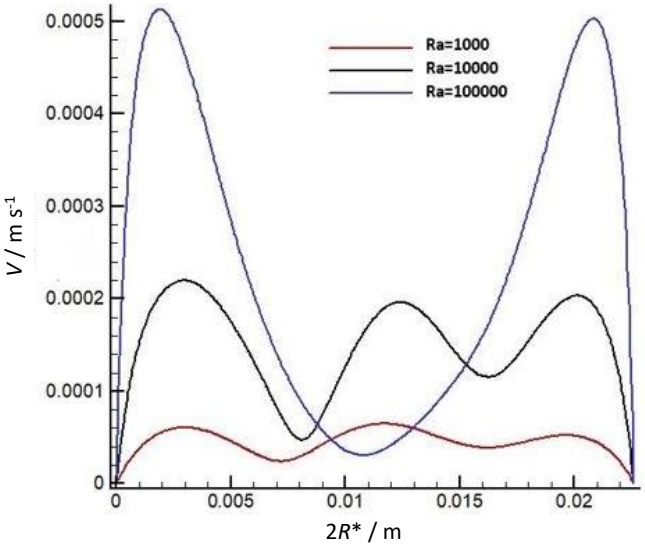

Figure 11. Velocity (V) along the vertical centerline for different Rayleigh numbers at Et = 10^{10} and Pr = 10

Figure 12 depicts the steady-state velocity values along the vertical centerline of the cavity for different elasticity moduli at Ra = 10^5 and Pr = 10. As can be seen, the elastic modulus has a negligible effect on fluid velocity. It is worth noting that the fluid velocity decreases at the maximal deformation of the flexible fin.

Figure 13 illustrates the maximum stress values with the deformation of the flexible fin for different Rayleigh numbers at Et = 10^{10} and Pr = 10. As observed, the maximum deformation of the fin increases by increasing the Rayleigh number. This finding is due to the augmented effect of the natural convective flow. Also, at a low Rayleigh number natural convective heat transfer is reduced and values of maximum deformation become lower.

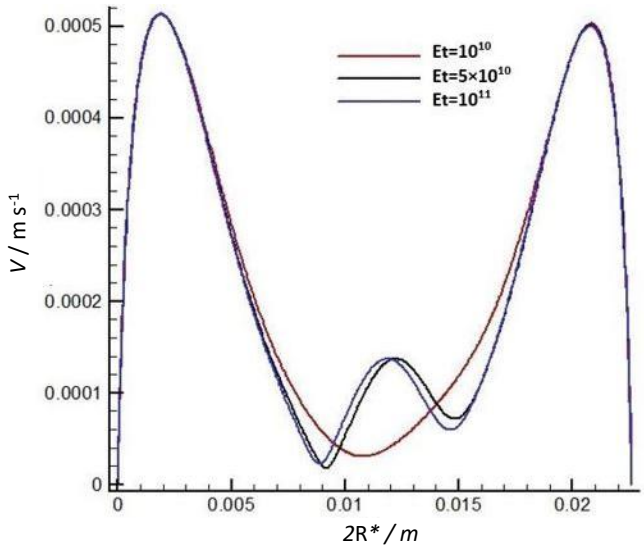

Figure 12. Velocity (V) along the vertical centerline for different elasticity modulus at Ra = $10^5$and Pr = 10.

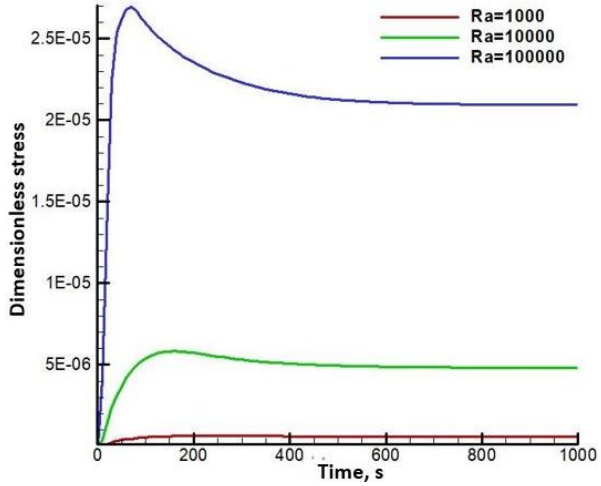

Figure 13. Maximal stress values of the flexible fin for different Rayleigh numbers at Et = 10^{10} and Pr = 10

Figure 14 shows the maximum stress values with the deformation of the flexible fin for different elasticity moduli at Ra = 10^5 and Pr = 10. The maximum deformation of the fin increases as the elasticity modulus is decreased, resulting in a greater degree of flexibility and higher overall maximal deformation. When the elasticity modulus increases, the fin becomes more rigid, and the maximal deformation decreases.

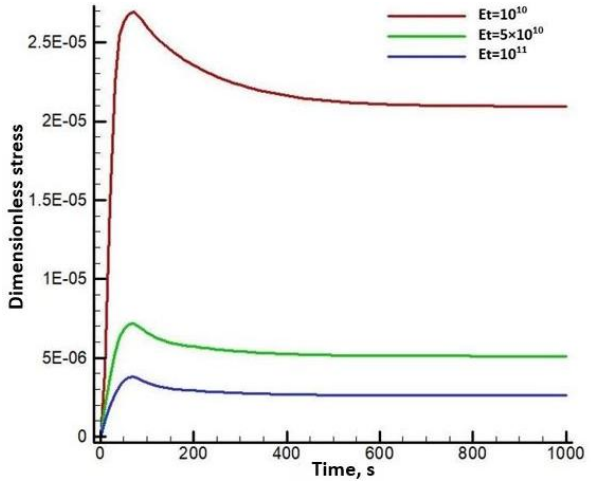

Figure 14. Maximal deformation stress values of the flexible fin over time for different elasticity modulus at Ra = $10^5$and Pr = 10.

Figure 15 illustrates the impact of the fin length on the stress with the deformation of the flexible fin overtime at Et = 10^{10} and Ra = 10^5. It has been observed that the stress and deformation of the fin increase as the fin length is increased.

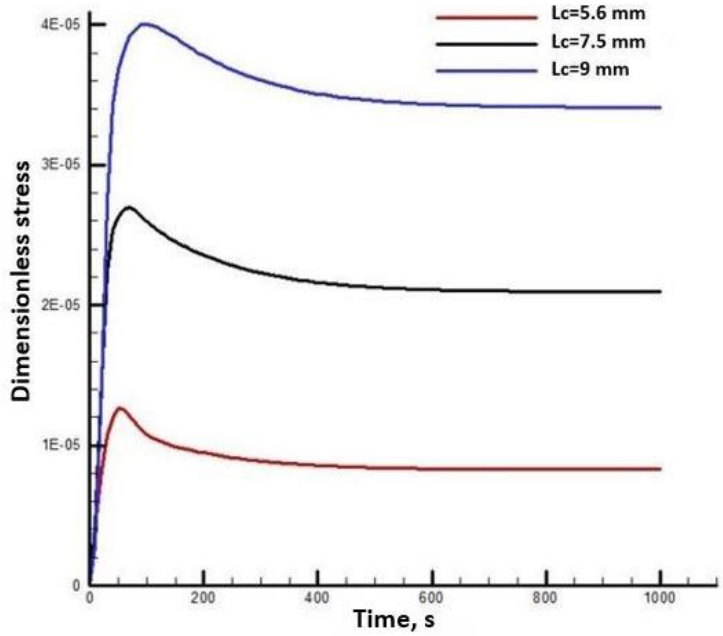

Figure 15. Maximum stress values of the flexible fin over time for different fin lengths (Lc) at Ra = 10^5 and Et = 10^{10}

Figure 16 depicts the Nusselt number along the hot wall over time for different fin positions (left side, right side, and top side) at Et = 10^{10} and Ra = 10^5. As can be seen, attachment of the fin at the top of the cavity has an improving impact on the heat transfer. It is worth noting that the left (hot wall) and right (cold wall) positions of the fin have the same effects on heat transfer.

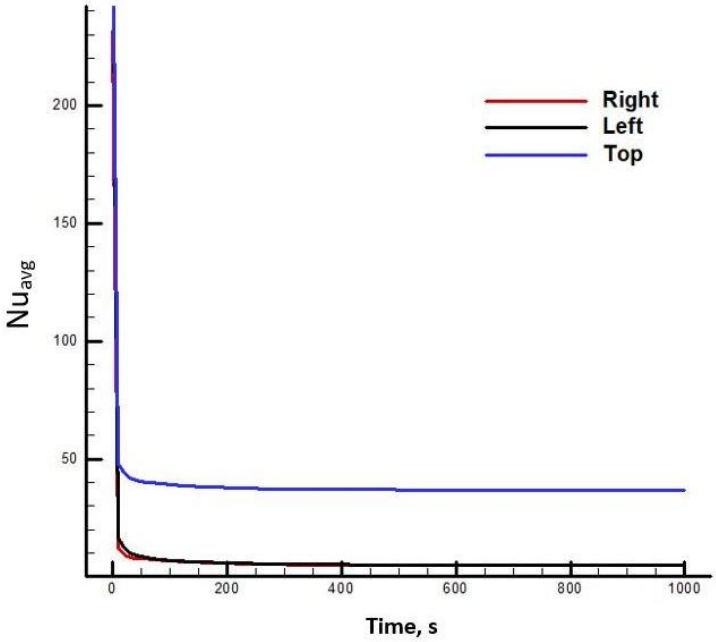

Figure 16. The average Nusselt number along the hot wall over time for different fin positions at Et = 10^{10} and Ra = 10^5

Figure 17 represents the fin maximal stress over time for different fin positions at Ra = 10^5 and Et = 10^{10}. The right fin position shows the maximal deformation stress, while the top position results in the lowest fin deformation stress.

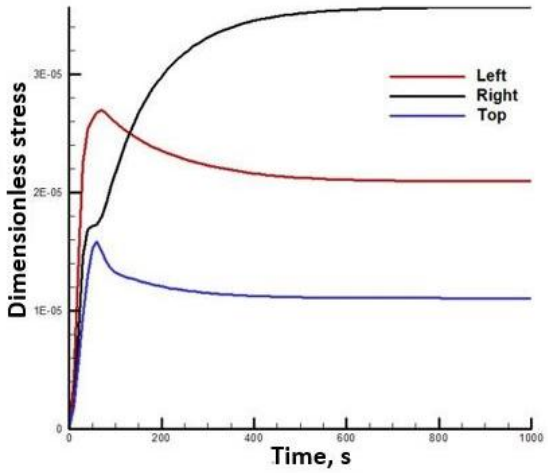

Figure 17. Maximum stress values of the flexible fin over time for different fin positions at Ra = 10^5 and Et = 10^{10}

5. CONCLUSION

Numerical investigations have been carried out on natural convective flow for Newtonian fluids in a circular enclosure using the finite elements method. The influences of the Rayleigh number (Ra) and elasticity modulus (Et) on the convective flow and heat transfer have been examined and discussed. Summary of the major results is as follows.

- Conduction is the primary mode of heat transfer in the early stages, but it gradually converts to natural convection. For higher Rayleigh numbers, the effects of the buoyancy force on vortices that form in the cavity are most important.
- The highest deformation of the fin is observed at the steady state when the fin elasticity modulus is low. Still the elasticity modulus does not affect the average Nusselt number on the hot wall.
- The increase in the Rayleigh number causes an increase in the convective flow intensity and heat transfer,
- It may be deduced that the placement of the fin on the top of the cavity improves heat transfer.

REFERENCES

[1] Turkyilmazoglu M. Exponential nonuniform wall heating of a square cavity and natural convection. *Chin J Phys*. 2022; 77: 2122-2135.https://dx.doi.org/10.1016/j.cjph.2021.12.021

[2] Mehryan SAM, Ghalambaz M, Ismael MA, Chamkha AJ. Analysis of fluid-solid interaction in MHD natural convection in a square cavity equally partitioned by a vertical flexible membrane. *J Magn Magn*. 2016; 424: 161-173. https://dx.doi.org/10.1016/j.jmmm.2016.09.123

[3] Jamesahar I, Halambaz MG, Chamkha AJ. Fluid–solid interaction in natural convection heat transfer in a square cavity with a perfectly thermal-conductive flexible diagonal partition. *Int J Heat Mass Transf*. 2016; 100: 303-319. https://dx.doi.org/https://doi.org/10.1016/j.ijheatmasstransfer.2016.04.046

[4] Shahrestani AB, Alshuraiaan B, Izadi M. Combined natural convection-FSI inside a circular enclosure divided by a movable barrier. *Int Commun Heat Mass Transf*. 2021; 126: 105426. https://dx.doi.org/10.1016/j.icheatmasstransfer.2021.105426

[5] Ghalambaz M, Mehryan SAM, Alsabery AI, Hajjar A, Izadi M,Chamkha A. Controlling the natural convection flow through a flexible baffle in an L-shaped enclosure. *Meccanica*. 2020; 55: 1561-1584. https://dx.doi.org/10.1007/s11012-020-01194-2

[6] Ismael MA, Jasim HF. Role of the fluid-structure interaction in mixed convection in a vented cavity. *Int J Mech. Sci*. 2017; 135: 190-202. https://dx.doi.org/10.1016/j.ijmecsci.2017.11.001

[7] Sabbar WA, Ismael MA, Almudhaffar M. Fluid-structure interaction of mixed convection in a cavity-channel assembly of flexible wall. *Int J Mech. Sci*. 2018; 149: 73-83. https://dx.doi.org/10.1016/j.ijmecsci.2018.09.041

[8] Alsabery AI, Selimefendigil F, Hashim I, Chamkha AJ, Ghalambaz M. Fluid-structure interaction analysis of entropy generation and mixed convection inside a cavity with flexible right wall and heated rotating cylinder. *Int J Heat Mass Transf*. 2019; 140: 331-345. https://dx.doi.org/10.1016/j.ijheatmasstransfer.2019.06.003

[9] Alsabery AI, Sheremet MA, Ghalambaz M, Chamkha AJ, Hashim I. Fluid-structure interaction in natural convection heat transfer in an oblique cavity with a flexible oscillating fin and partial heating. *Appl Therm Eng*. 2018; 145: 80-97. https://dx.doi.org/10.1016/j.applthermaleng.2018.09.039

[10] Ghalambaz M, Jamesahar E, Ismael MA, Chamkha AJ. Fluid-structure interaction study of natural convection heat transfer over a flexible oscillating fin in a square cavity. *Int J Therm Sci*. 2016; 111: 256-273. https://dx.doi.org/10.1016/j.ijthermalsci.2016.09.001
[11] Saleh H, Naganthran K, Hashim I, Ghalambaz M, Nazar R. Role of fluid-structure interaction in free convection in square open cavity with double flexible oscillating fins. *Alex Eng J*. 2021; 61: 1217-1234. https://dx.doi.org/10.1016/j.aej.2021.04.073
[12] Raisi A, Arvin I. A numerical study of the effect of fluid-structure interaction on transient natural convection in an air-filled square cavity. *Int J Therm Sci*. 2018; 128: 1-14. https://dx.doi.org/10.1016/j.ijthermalsci.2018.02.012
[13] Khanafer K, Vafai K. Effect of a circular cylinder and flexible wall on natural convective heat transfer characteristics in a cavity filled with a porous medium. *Appl Therm Eng*. 2020; 181: 115989. https://dx.doi.org/10.1016/j.applthermaleng.2020.115989
[14] Khalil WH, Azzawi IDJ, Al-damook A. The optimisation of MHD free convection inside porous trapezoidal cavity with the wavy bottom wall using response surface method. *Int Commun Heat Mass Transf*. 2022; 134: 106035. https://dx.doi.org/10.1016/j.icheatmasstransfer.2022.106035
[15] Moria H. Natural convection in an L-shape cavity equipped with heating blocks and porous layers. *Int Commun Heat Mass Transf*. 2021; 126: 105375. https://dx.doi.org/10.1016/j.icheatmasstransfer.2021.105375
[16] Saleh H, Hashim I, Jamesearl E, Ghalambaz M. Effects of flexible fin on natural convection in enclosure partially-filled with porous medium. *Alex Eng J*. 2020; 59: 3515-3529. https://dx.doi.org/10.1016/j.aej.2020.05.034
[17] Mehryan SAM, Alsabery A, Modir A, Izadpanahi E, Ghalambaz M. Fluid-structure interaction of a hot flexible thin plate inside an enclosure. *Int J Therm Sci*. 2020; 153: 106340. https://dx.doi.org/10.1016/j.ijthermalsci.2020.106340
[18] Savio RR, Shaik S, Kumar RS. Numerical study of natural convection around a square cylinder within a square enclosure for different orientations. *J Therm Anal Calorim*. 2021; 147: 1711-1725. https://dx.doi.org/10.1007/s10973-020-10499-z
[19] Subhani S, Kumar RS. Natural Convection Heat Transfer Enhancement of Circular Obstacle within Square Enclosure. *J Therm Anal Calorim*. 2021; 147: 4711-4729. https://dx.doi.org/10.1007/s10973-021-10829-9
[20] Pal GC, Nammi G, Pati S, Randive PR, Baranyi L. Natural convection in an enclosure with a pair of cylinders under magnetic field. *Case Stud Therm Eng*. 2022; 30: 101763. https://dx.doi.org/10.1016/j.csite.2022.101763
[21] Long T, Huang C, Hu D, Liu M. Coupling edge-based smoothed finite element method with smoothed particle hydrodynamics for fluid structure interaction problems. *Ocean Eng*. 2021; 225: 108772. https://dx.doi.org/10.1016/j.oceaneng.2021.108772
[22] Hakim MdA, Ahad AI, Karim AUl, Saha S, Hasan MN. Fluid structure interaction and heat transfer enhancement with dynamic flexible flow modulator. *Int Commun Heat Mass Transf*. 2022; 134: 105983. https://dx.doi.org/10.1016/j.icheatmasstransfer.2022.105983
[23] Gilmanov A, Le TB, Sotiropoulos FA. Numerical approach for simulating fluid structure interaction of flexible thin shells undergoing arbitrarily large deformations in complex domains. *J Comput Phys*. 2015; 300: 814-843. https://dx.doi.org/10.1016/j.jcp.2015.08.008
[24] Shahabadi M, Mehryan SAM, Ghalambaz M, Ismael M. Controlling the natural convection of a non-Newtonian fluid using a flexible fin. *Appl Math Model*. 2020; 92: 669-686. https://dx.doi.org/10.1016/j.apm.2020.11.029
[25] Ghalambaz M, Mehryan SAM, Feeoj RK, Hajjar A, Hashim I, Mahan RB. Free convective heat transfer of a non-Newtonian fluid in a cavity containing a thin flexible heater plate: an Eulerian–Lagrangian approach. *J Therm Anal Calorim*. 2020; 147: 1809-1824. https://dx.doi.org/10.1007/s10973-020-10292-y
[26] Zadeh SMH, Mehryan SAM, Izadpanahic E, Ghalambaz M. Impacts of the flexibility of a thin heater plate on the natural convection heat transfer. *Int J Therm Sci*. 2019; 145: 106001. https://dx.doi.org/10.1016/j.ijthermalsci.2019.106001
[27] Sairamu M, Chhabra RP. Natural convection in power-law fluids from a tilted square in an enclosure. *Ocean Eng*. 2012; 56: 319-339. https://dx.doi.org/j.ijheatmasstransfer.2012.09.033
[28] Turan O, Sachdeva A, Chakraborty N, Poole RJ. Laminar natural convection of power-law fluids in a square enclosure with differentially heated side walls subjected to constant temperatures. *J Non-Newton Fluid Mech*. 2011; 166: 1049-1063. https://dx.doi.org/10.1016/j.jnnfm.2011.06.003
[29] Su ZG, Li TF, Luo K, Wu J, Yi HL. Electro-thermo-convection in non-Newtonian power-law fluids within rectangular enclosures. *J Non-Newton Fluid Mech*. 2020; 288: 2122-2135. https://dx.doi.org/10.1016/j.jnnfm.2020.104470
[30] Salehpour A, Sadatlub MA, Sojoudi A. Unsteady Natural Convection in a Differentially Heated Rectangular Enclosure Possessing Sinusoidal Corrugated Side Walls Loaded with Power Law Non-Newtonian Fluid. *Fluid Dyn*. 2019; 54: 159-176. https://dx.doi.org/10.1134/S0015462819010129
[31] Gangawane KM, Manikandan B. Laminar natural convection characteristics in an enclosure with heated hexagonal block for non-Newtonian power-law fluids. *Chin J Chem Eng*. 2016; 25: 555-571. https://dx.doi.org/10.1016/j.cjche.2016.08.028
[32] Zhou X, Sun Z. Numerical investigation of non-Newtonian power-law flows using B-spline material point method. *J Non-Newton Fluid Mech*. 2021; 298: 104678. https://dx.doi.org/10.1016/j.jnnfm.2021.104678
[33] Pandey S, Cho HW, Choi HK, Park YG, Seo YM, Ha MY. Thermal and flow characteristics of buoyancy-driven non-Newtonian flows at a high Rayleigh number of 10^7 and predictions from an artificial neural network. *J Mech Sci Technol*. 2021;35: 1791-1805. https://dx.doi.org/10.1007/s12206-021-0341-6
[34] KebritiS, Moqtaderi H. Numerical simulation of convective non-Newtonian power-law solid-liquid phase change using the lattice Boltzmann method. *Int J Therm Sci*. 2020; 159: 106574. https://dx.doi.org/10.1016/j.ijthermalsci.2020.106574
[35] Jain SR, Subhani S, Kumar, RS. Numerical study on performance enhancement of a square enclosure with a circular cylinder of varying geometries. *J Therm Anal Calorim*. 2021; 147: 2579-2599. https://dx.doi.org/10.1007/s10973-021-10641-5

[36] Loenko DS, Shenoy A, Sheremet MA. Effect of time-dependent wall temperature on natural convection of a non-Newtonian fluid in an enclosure. Ocean Eng. 2021; 166: 319-339. https://dx.doi.org/10.1016/j.ijthermalsci.2021.106973
[37] Abdulkadhim A, Abed IM, Said NM. Review of Natural Convection Within Various Shapes of Enclosures. Arab J Sci Eng. 2021; 46: 11543-11586. https://dx.doi.org/10.1007/s13369-021-05952-6
[38] Yang P, Huang C, Zhang Z, Long T, Liu M. Simulating natural convection with high Rayleigh numbers using the Smoothed Particle Hydrodynamics method. *Int J Heat Mass Transf*. 2020; 166: 2122-2135. https://dx.doi.org/10.1016/j.cjph.2021.12.021

Numeričko ispitivanje slobodne konvekcije unutar kružne šupljine sa fleksibilnim perajem

Atika Bencherif[1], Mohamed Bouzit[1], Abderrahim Mokhefi[2], Hanaa Derraz[1] i Fatima Zohra Khelif[1]

[1]Laboratory of Maritime Sciences and Engineering LSIM Faculty of Mechanical Engineering, University of Science and Technology of Oran Mohamed Boudiaf, Oran, Algeria
[2]Mechanics, Modeling and Experimentation Laboratory L2ME, Faculty of Sciences and Technology, Bechar University, Bechar, Algeria

(Naučni rad)

Izvod

U ovom radu numerički je proučavan problem nestalne prirodne konvekcije unutar kružne šupljine koja sadrži fleksibilno peraje. Leva strana šupljine je vruća, dok je desna hladna. Fleksibilno elastično peraje je pričvršćeno za centar vrućeg zida. Interakcija fluida i strukture u šupljini i fleksibilnim perajem je kombinovana sa Njutnovim fluidom. Glavne jednačine interakcije fluid-fleksibilna peraja su rešene primenom metode konačnih elemenata i proizvoljnog Lagranž-Eulerovog pristupa. U ovoj studiji ispitivani su efekti elastičnog fleksibilnog peraja na prirodnu konvekciju unutar kružnih šupljina. Rejlijev broj ($10^3 \leq Ra \leq 10^5$) i modul elastičnosti ($10^{10} \leq Et \leq 10^{11}$) su parametri koji su ispitivani, kao i prosečni Nuseltovi brojevi i izoterme i strujne linije. Rezultati pokazuju da povećanje Relejovog broja izaziva povećanje prosečnog Nuseltovog broja, koji postaje značajan za veći Rejlijev broj. Time je otkriveno da kružni oblik šupljine može poboljšati brzinu prenosa toplote.

Ključne reči: Njutnovski fluid; interakcija fluid-struktura; metoda konačnih elemenata; modul elastičnosti; prosečan Nuseltov broj; Rejlijev broj